

2

AD-A208 661

OFFICE OF NAVAL RESEARCH

Contract N00014-84-K-0052

Task No. NR 051-855

Technical Report No. 21

Analytical Utility of Cylindrical Microelectrodes

by

Scott T. Singleton, John J. O'Dea, and Janet Osteryoung

Prepared for Publication

in

Analytical Chemistry

State University of New York at Buffalo  
Department of Chemistry  
Buffalo, New York 14214

May 31, 1989

Reproduction in whole or in part is permitted for  
any purpose of the United States Government.

This document has been approved for public release  
and sale; its distribution is unlimited.

DTIC  
ELECTE  
JUN 05 1989  
S H D

89 6 05 093

REPORT DOCUMENTATION PAGE				Form Approved OMB No 0704-0188	
1a REPORT SECURITY CLASSIFICATION UNCLASSIFIED		1b RESTRICTIVE MARKINGS			
2a SECURITY CLASSIFICATION AUTHORITY		3 DISTRIBUTION/AVAILABILITY OF REPORT Approved for public release and sale. Distribution unlimited.			
2b DECLASSIFICATION/DOWNGRADING SCHEDULE					
4. PERFORMING ORGANIZATION REPORT NUMBER(S) ONR Technical Report 21		5 MONITORING ORGANIZATION REPORT NUMBER(S)			
6a NAME OF PERFORMING ORGANIZATION Department of Chemistry	6b OFFICE SYMBOL (If applicable)	7a. NAME OF MONITORING ORGANIZATION			
6c. ADDRESS (City, State, and ZIP Code) State University of New York at Buffalo Buffalo, New York 14214		7b ADDRESS (City, State, and ZIP Code)			
8a. NAME OF FUNDING / SPONSORING ORGANIZATION Office of Naval Research	8b. OFFICE SYMBOL (If applicable) ONR	9 PROCUREMENT INSTRUMENT IDENTIFICATION NUMBER N00014-84-K-0052			
8c. ADDRESS (City, State, and ZIP Code) Chemistry Program Arlington, Virginia 22217		10 SOURCE OF FUNDING NUMBERS			
		PROGRAM ELEMENT NO	PROJECT NO	TASK NO	WORK UNIT ACCESSION NO
				NR-051-855	
11 TITLE (Include Security Classification) Analytical Utility of Cylindrical Microelectrodes					
12 PERSONAL AUTHOR(S) Scott T. Singleton, John J. O'Dea, and Janet Osteryoung					
13a TYPE OF REPORT Technical	13b TIME COVERED FROM _____ TO _____	14 DATE OF REPORT (Year, Month, Day) 1989 May 31	15 PAGE COUNT		
16 SUPPLEMENTARY NOTATION					
17 COSATI CODES			18 SUBJECT TERMS (Continue on reverse if necessary and identify by block number)		
FIELD	GROUP	SUB-GROUP	cylindrical electrodes, voltammetry, square wave voltammetry, stripping analysis, microelectrodes, platinum, (mgm)		
19 ABSTRACT (Continue on reverse if necessary and identify by block number)					
<p>The behavior and utility of a platinum microelectrode is demonstrated for the cylindrical geometry. The working electrode used here is a small platinum wire (25 <math>\mu</math>m in diameter and 0.5 to 1.0 cm in length) which is sealed in a 20 <math>\mu</math>L glass microcapillary pipet. Mass transport to a stationary cylinder in quiescent solution is governed by axi-symmetrical cylindrical diffusion. Various experiments (chronoamperometry and cyclic staircase and square-wave voltammetry) were performed on the ferricyanide/ferrocyanide couple which was chosen as a reversible system. The theory is presented for cyclic staircase and for square-wave voltammetry. The electrode exhibited the predicted behavior in these experiments. Plating and stripping of silver illustrates the practicality of this electrode, especially as employed with square-wave voltammetry.</p>					
20 DISTRIBUTION/AVAILABILITY OF ABSTRACT <input type="checkbox"/> UNCLASSIFIED/UNLIMITED <input checked="" type="checkbox"/> SAME AS RPT <input type="checkbox"/> DTIC USERS			21 ABSTRACT SECURITY CLASSIFICATION UNCLASSIFIED		
22a NAME OF RESPONSIBLE INDIVIDUAL			22b TELEPHONE (Include Area Code)	22c OFFICE SYMBOL	

ANALYTICAL UTILITY OF CYLINDRICAL MICROELECTRODES

by

Scott T. Singleton, John J. O'Dea

and

Janet Osteryoung\*

Department of Chemistry  
State University of New York at Buffalo  
Buffalo, NY 14214

BRIEF

Staircase and square-wave voltammetry at a cylinder are treated experimentally and theoretically.

ABSTRACT

The behavior and utility of a platinum microelectrode is demonstrated for the cylindrical geometry. The working electrode used here is a small platinum wire (25  $\mu\text{m}$  in diameter and 0.5 to 1.0 cm in length) which is sealed in a 2  $\mu\text{L}$  glass microcapillary pipet. Mass transport to a stationary cylinder in quiescent solution is governed by axi-symmetrical cylindrical diffusion. Various experiments (chronoamperometry and cyclic staircase and square-wave voltammetry) were performed on the ferri-ferrocyanide couple which was chosen as a reversible system. The theory is presented for cyclic staircase and for square-wave voltammetry. The electrode exhibited the predicted behavior in these experiments. Plating and stripping of silver illustrates the practicality of this electrode, especially as employed with square-wave voltammetry.



Accession For	
NTIS GRA&I	<input checked="" type="checkbox"/>
DTIC TAB	<input type="checkbox"/>
Unannounced	<input type="checkbox"/>
Justification	
By _____	
Distribution/	
Availability Codes	
Dist	Avail and/or Special
A-1	

Microelectrodes in general possess advantageous properties which can be exploited in various experimental applications (1,2). The small size of these electrodes results in a decrease in capacity current as well as an increase in faradaic current density due to nonplanar diffusion of material to the electrode surface. The small total current which flows reduces the problem of ohmic drop through the electrolyte (3). With these attributes, experiments are possible at microelectrodes which cannot be performed at large electrodes. For example, microelectrodes can be used in highly resistive media (4,5), and the kinetics of fast reactions (6,7) can be studied due to the diminution of capacity currents and IR drop.

A cylindrical microelectrode appears to be a conveniently constructed working electrode for use in electrochemical studies. Such a microelectrode can be readily manufactured from available metal wire or from carbon fibers. In fact, the platinum microcylinder used herein can be constructed in approximately fifteen minutes. Once made, such devices are easily cleaned by insertion into a flame or by immersing in an appropriate cleaning solution, after which they are ready for use.

It is important to notice that in comparison with other geometries (e.g., disks), no polishing or other tedious fabrication procedure is necessary. The seal between the insulator and the conductor is a minor determinant of overall performance. The area of the cylinder depends not only on its radius but also on its length. Therefore, one can adjust the length of the microcylinder to achieve the desired magnitude of current without changing the diffusional characteristics (8). Thus, enhanced diffusional flux can be realized without requiring the measurement of small current signals against noisy backgrounds.

Despite these salient features, microcylinder electrodes have not been so extensively used as working electrodes in comparison with other microelectrode

geometries (e.g., disks, lines, spheres, etc.). This is partly a consequence of the difficulty in the theoretical treatment of cylindrical diffusion (9). However, with the establishment of theoretical expressions for various electrochemical techniques at microcylinder electrodes by Aoki, et al. (10-13), the mathematical objection to such electrodes becomes less of an inhibition. Here we extend the treatment of Aoki, et al. to cyclic staircase and square-wave voltammetry.

A second drawback to cylindrical electrodes is the rather awkward time dependence displayed by the chronoamperometric response, the details of which are discussed below. This dependence makes the conventional experiment difficult to interpret by conventional means. The present work is intended to demonstrate that for usual analytical purposes, square-wave voltammetry at microcylinders does not display any inconvenient distortions in shape or potential due to cylindrical diffusion (14-16). Furthermore, exact analysis of the shapes of voltammograms can be carried out by means of the COOL algorithm (17) described below without needing to resort to the complex methods of analysis described by Aok., et al. (10-13).

Finally, in the case of anodic stripping voltammetry, for practical convenience it is desired that a stripping peak current (or charge) be directly proportional to deposition time. Although the limiting current at a stationary cylinder depends on time, over the numerical ranges of interest the deposition charge is linear in time to an acceptable degree of accuracy as shown below.

The potential-time waveform employed in cyclic staircase voltammetry involves a series of potential pulses of amplitude  $\Delta E_s$  and width (duration)  $t_p$  (or frequency  $f = 1/t_p$ ). Beginning at an initial potential  $E_1$  sufficiently distant from the half-wave potential of the analyte such that no faradaic

reaction occurs, the scan proceeds toward a switching potential at which  $\Delta E_s$  is replaced by  $-\Delta E_s$  to return to  $E_i$ . On each step, the current is measured at the end of the potential pulse.

In the case of square-wave voltammetry, a square wave is superimposed upon a base staircase potential (16). Such a waveform can be characterized by  $\Delta E_s$ , the step height of the staircase,  $E_{sw}$ , the square-wave amplitude (half the peak to peak value), and  $t_p$ , the pulse width ( $t_p = 1/2f$ ,  $f$  = frequency of the staircase). The characteristic time parameter for the experiment is chosen to be the pulse width rather than the period of the square wave in order to make the proper comparison with the chronoamperometric experiment.

The current is measured at the end of each forward and reverse pulse of the square wave. The analytical signal is defined to be the net (or difference) current,  $i = i_f - i_r$ , which is plotted against the base staircase potential. A symmetrical bell-shaped curve positioned at the reversible half-wave potential results for a Nernstian system.

The potential-time waveform can be described by

$$E_j = E_i \mp \text{INT}((j+1)/2)\Delta E_s \pm (-1)^j E_{sw} \quad (1)$$

in which the upper sign is chosen for scans in the negative direction, the lower for scans in the positive direction, INT indicates the integer part of the quantity, and  $E_j$  is the potential on the  $j^{\text{th}}$  half cycle of the square wave. The resulting measured current can be expressed by:

$$i_j = nFAC(D/\pi t_p)^{1/2} \psi_j \quad (2)$$

where  $i_j$  is the current on the  $j^{\text{th}}$  half cycle of the square wave,  $n$  the number of electrons transferred,  $F$  the value of the Faraday,  $A$  the electrode area,  $D$  the diffusion coefficient of the reactant,  $C$  the bulk concentration of reactant, and  $\psi_j$  the dimensionless current function.

In the case of a reversible couple subject to semi-infinite linear diffusion (16):

$$\psi_j = \sum_{k=1}^j (Q_{k-1} - Q_k) / (j - k + 1)^{1/2} \quad (3)$$

where  $Q_j$  is the fraction concentration of reactant at the electrode surface ( $C_0^S / (C_0^S + C_R^S)$  for reductions) calculated from the Nernst equation:

$$Q_j = (1 + \exp(\pm nF(E_j - E_{1/2})/RT))^{-1} \quad (4)$$

where the - and + signs are chosen for reductions and oxidations, respectively,  $F/RT = 38.92 \text{ V}^{-1}$  at  $25^\circ\text{C}$ ,  $E_{1/2}$  is the reversible half-wave potential, and  $Q_0$  is by definition unity. For a reversible couple at an electrode of arbitrary geometry (14):

$$\psi_j = (\pi t_p / D) \left\{ \sum_{k=1}^j (Q_{k-1} - Q_k) R_{j-k+1}(\theta) \right\} \quad (5)$$

In eq 5,  $R_j$  is the properly normalized solution to the chronoamperometric problem, (e.g.,  $R_j = (D/j\pi t_p)^{1/2}$  for the planar case). Aoki, et al. have shown that for a cylinder the function  $R_j$  can be approximated by (11):

$$R_j(\theta) = (D/r) \left( \frac{1}{(\pi j \theta)^{1/2}} + 0.422 - 0.0675 \log(j\theta) \pm 0.0058 \left\{ \log(j\theta) - 1.47 \right\}^2 \right) \quad (6)$$

where  $r$  is the electrode radius,  $\theta = Dt_p/r^2$  and the plus sign is chosen for  $\log(j\theta) \geq 1.47$ , minus for  $\log(j\theta) < 1.47$ .

The values of the current  $i_j$  when  $j$  is even comprise the forward current  $i_f$ , while those when  $j$  is odd comprise the reverse current  $i_r$ . The net current is the difference  $i_f - i_r$  for each step of the staircase.

These same equations (2-6) also can be used to calculate cyclic staircase voltammograms with the modification that the potential-time waveform is described for  $m$  total steps as:

$$E_j = E_i - j\Delta E_s \quad (7)$$

for the first  $m/2$  steps of the staircase and by:

$$E_j = (E_i - (m/2)\Delta E_s) + (j - m/2 + 1)\Delta E_s \quad (8)$$

for steps  $(m/2 + 1)$  to  $m$ . The above formulation applies to cathodic scans. The + and - signs are reversed for all but the  $(j - (m/2 + 1))$  term in eq 8 in order to obtain the analogous waveform for an anodic scan.

For a single potential step from  $E_i \gg E_{1/2}$  (for reductions) to the diffusion-limited plateau ( $E \ll E_{1/2}$  for reductions) at a cylinder, combining eqns 2, 4, and 5 yields the chronoamperometric result

$$i = nFACR(\theta) \quad (9)$$

At longer times the chronoamperometric response can be approximated by (18):

$$i = 2nFADC/r \ln(4\theta) \quad (10)$$

The quantity  $\theta = Dt/r^2$  in eqns 5, 6, 9, and 10 characterizes the diffusional regime. For sufficiently short times or large radii  $\theta \ll 1$  and the diffusion is planar (only the leading term need be considered). With decreasing radius or longer times, cylindrical diffusion becomes more important. For the present case ( $r = 12.5 \mu\text{m}$ ), the Cottrell equation (eq 2 with  $\psi_j = 1$ ) is obeyed within 2% for  $t < 5$  ms and the limiting expression (eq 10) applies within 2.5% for  $t > 2$  s.

#### EXPERIMENTAL SECTION

The experiments were performed in a standard three electrode configuration in an IBM cell. The homemade platinum wire microcylinder electrode served as the working electrode and was accompanied by a commercial saturated calomel reference electrode and a platinum wire auxiliary electrode. In the case of anodic stripping of silver, the reference electrode was placed in a salt bridge containing 1.00 M  $\text{KNO}_3$ . All potentials were measured and are reported with respect to the SCE reference. This cell was used in conjunction with an EG&G PARC 273 potentiostat which was connected to a DEC PDP 8/e computer through the RS-232 interface. Computer programs written in Fortran IV were used to control experiments, acquire and analyze data, and store the data on magnetic disks.

The ferri-ferrocyanide couple was chosen as a reversible system for use in the investigations. Solutions were made with deionized water prepared by passing distilled water through a Millipore Milli-Q purification system.

Solutions were purged before the experiments by passing purified argon gas through the solution for ten to fifteen minutes. Residual traces of oxygen in the gas were removed by passing the argon through a BASF copper catalyst. The gas was saturated with water vapor by means of a gas washing bottle containing deionized water through which the argon was bubbled before it was introduced into the cell. The solution was blanketed with argon during each experiment. The entire cell was thermostated at 25 C with a circulating water bath.

The working electrode was constructed by means of the following procedure. A length of platinum wire 25  $\mu\text{m}$  in diameter (Aesar, Johnson Matthey, Inc.) was inserted into a Drummond 2  $\mu\text{L}$  glass microcapillary pipet. The tip of the pipet was sealed in a cool flame. The electrical connection was made by soldering a silver-plated copper wire at the far end. To ensure a sound mechanical connection, the joint was further sealed in a piece of heat shrinkable tubing. The exposed tip of the electrode is a negligible fraction of the total surface area (0.063% for a 1 cm length of wire).

Pretreatment of the working electrode was found to be crucial for obtaining ideal response (19). An electrode was cleaned by inserting it into a solution of 0.5 g potassium dichromate dissolved in 50 mL concentrated sulfuric acid for approximately 30 minutes. After rinsing in deionized water, the electrode was introduced into the cell. This cleaning solution oxidatively destroys grease, dust, and other organic materials on the electrode. It also yields a heavily oxidized platinum surface. This surface oxide is then reduced in the electrochemical cell by means of a potential pretreatment. The potential was held at a value of -1.0 V for 10 seconds, after which the potential was cycled from 1.2 V to -1.0 V in a cyclic staircase waveform ( $\Delta E_s = 25 \text{ mV}$ ,  $f = 10 \text{ Hz}$ ). This potential hold and cycle treatment was applied five times prior to each experiment. The response of

the electrode was found to deteriorate rapidly with several successive experiments. Wholly unsatisfactory behavior was observed unless the potential cycling was applied prior to each experiment. Typically, the results would exhibit a higher than theoretically predicted magnitude of current for a given potential pulse. Following the potential pretreatment, the electrode was held at the initial potential of the experiment at hand for 30 seconds and the solution was agitated with the bubbling of argon gas for the first few seconds in order to eliminate any concentration gradients.

In the case of silver stripping, the potential cycling was applied in the background electrolyte only (1.00 M  $\text{KNO}_3$ ) prior to each series of experiments. The potential was then held at +0.5 V between experiments. Plating of silver onto platinum was carried out at a potential of 0 V for 15 s in the absence of mechanical stirring. Anodic dissolution of silver was accomplished by scanning from 0 V to +0.5 V using square-wave voltammetry.

The diffusion coefficient for ferricyanide in 1.00 M  $\text{KNO}_3$  was found to be  $7.3 \times 10^{-6} \text{ cm}^2/\text{s}$  by chronoamperometric measurement at a platinum disk 0.8 cm in diameter. This value agrees well with the value of  $7.63 \times 10^{-6} \text{ cm}^2/\text{s}$  obtained by von Stackelberg, et al. (20).

Experiment was compared with theory by means of the COOL algorithm (17), which finds the best-fitting theoretical curve by means of a non-linear least-squares method equivalent to the method of maximum likelihood. The procedure is as follows. The experimental current is considered to be a linear function of the theoretical dimensionless current,  $i_{\text{exp}} = a + b \psi_{\text{th}}$ . The best-fitting line is that which minimizes the quantity  $(1-R)$ , where R is the correlation coefficient of the linear regression of  $i_{\text{exp}}$  on  $\psi_{\text{th}}$ . Initial guesses for the parameters sought and initial step sizes are used to begin a simplex search according to the modified simplex algorithm (21) for the optimal values of the

parameters, which are those which minimize  $(1-R)$ . The optimum is considered to be reached when successive values of the parameters agree within 0.01% in each dimension.

## RESULTS AND DISCUSSION

Chronoamperometry was performed on a solution of  $K_4Fe(CN)_6$  with a cylindrical platinum electrode with the resulting current-time transient as shown in Figure 1. Also shown is the Cottrell current calculated for an electrode of the same area. Note the increase in current density at the microelectrode due to non-planar diffusion of material to the electrode surface. The current-time response resulting from such a potential step at an electrode subject to cylindrical diffusion calculated from eqns 6 and 9 also appears in Figure 1. The absolute agreement between theory and experiment is excellent.

Equation 10 shows that the diffusion-limited current at a cylinder should decrease steadily with time. Experimentally this is not observed. Also the experimental currents at long times are substantially larger than those predicted by eq 10. For example, in a typical experiment similar to that of Figure 1, the current predicted by eq 10 for  $\tau = 300$  s was 1.24  $\mu A$  whereas the experimental current, substantially time-independent, was 2.04  $\mu A$ . This is presumably the result of natural convection. Laitinen and Kolthoff observed this phenomenon at platinum wire electrodes of  $2.5 \times 10^{-2}$  cm radius while performing "steady state" voltammetry of various analytes (22,23). The predicted charge-time curve can be obtained by integrating eq 9; this is displayed and compared with experiment in Figure 2. The best straight line fit to the theoretical curve over the range 9-300 s is described by  $q = a+bt$  where  $a = 0.367$   $\mu C$ ,  $b = 1.332$   $\mu A$  with correlation coefficient 0.9992. The corresponding values for the experimental curve over the range 1-300 s are 0.112  $\mu C$ , 2.156  $\mu A$ , and 0.99997. The well-behaved charge-time response bodes well for stripping voltammetry, in which one wishes to achieve a reproducible

preconcentration step. The enhanced current density at microcylinders offers the possibility of a deposition step with no mechanical stirring required.

Staircase and square-wave voltammetry. A series of cyclic staircase voltammograms was obtained for various concentrations of  $K_3Fe(CN)_6$ . From the heights of the forward peaks for the reduction of ferricyanide (background subtracted), calibration curves were obtained as described below. Figure 3 depicts a cyclic staircase experiment for ferricyanide and the calculated response for the same system at a planar electrode of the same area. The effect of non-planar diffusion can be seen easily. The features of the voltammogram are substantially altered by the effect of the non-planar diffusion.

Also performed on the same solutions was a series of square-wave experiments. Figure 4 displays a typical square wave result together with the best-fitting theoretical curve for planar diffusion (eqns 2-4) and that calculated for a planar electrode of the same area (eqns 2-4). The best-fitting theoretical curve was found using the COOL algorithm. The shape and position on the potential scale of the experimental curve is seen to be exactly that of the curve which would be obtained at a planar electrode. The only effect of the cylindrical diffusion is to increase the current density (i.e., the sensitivity of the measurement). The cylindrical microelectrode simply yields the same net current response as a planar electrode of a larger area.

Calibrations carried out in the submillimolar to millimolar range of concentration yielded square-wave voltammograms similar to those of Figure 4. For the conditions of Figures 2-4, regression analysis for peak current with concentration yielded straight lines of correlation coefficient 0.999 and

slopes and y-intercepts respectively of 2.01  $\mu\text{A}/\text{mM}$  and 0.0091  $\mu\text{A}$  for staircase voltammetry and 4.90  $\mu\text{A}/\text{mM}$  and 0.0259  $\mu\text{A}$  for square-wave voltammetry.

In the case of planar diffusion, the current is proportional to square root of frequency (cf. eq 2). The relationship for cylindrical diffusion is far more complex. However, in a practical experimental situation, a test of  $i_p$  vs  $f^{1/2}$  at a cylinder will usually appear to be linear as well. This is illustrated in Figure 5 which shows net currents for frequency varied from 5 to 300 Hz together with theoretical curves for the cylinder and a plane of the same area. Note that although the relationship in Figure 5 is linear, the y-intercept of the experimental points is non-zero as a result of the non-planar diffusion. Background currents obtained in supporting electrolyte alone have been subtracted from the curves obtained for reduction of ferricyanide to obtain the voltammograms displayed in Figure 5. At higher frequencies and more negative potentials, this procedure overcorrects for background current and produces the negative current tails apparent in the inset. The peak currents were measured not with respect to zero, but rather with respect to a line drawn tangent to the voltammogram in potential regions before and after the peak.

The net peak position is invariant with respect to the frequency despite the geometry of the electrode. Moreover, the peak positions are all centered about 218 mV, the half-wave potential of the couple.

The full width at half height for the net current voltammograms is also unchanging with frequency. For a reversible electron transfer under these conditions (14):

$$W_{1/2} = (1/nf) \left( 3.53 + 3.46(nfE_{sw})^2 / (nfE_{sw} + 8.1) \right) \quad (12)$$

For  $T = 25^{\circ}\text{C}$  and  $E_{\text{sw}} = 50 \text{ mV}$ ,  $W_{1/2} = 124 \text{ mV}$ . This calculated result agrees well with the experimentally observed value of  $126 \text{ mV}$ . Thus, the net current voltammograms exhibit a height proportional to concentration, a peak position at the half-wave potential, and a full width at half height which can be used to determine the number of electrons transferred. Therefore, particularly with square-wave voltammetry, the easily constructed cylinder electrode proved to be an analytically useful indicator.

Although the shape of the net current square-wave voltammogram is unaffected by the cylindrical geometry, the individual forward and reverse currents do depend on the extent and nature of non-planar diffusion. Thus the individual forward and reverse currents at a cylinder can be compared with theory (given by eqns 2, 4-6) for a cylinder to obtain the parameters of the model, namely  $E_{1/2}$  and  $\sqrt{D/r}$ . A typical voltammogram together with the best fit obtained by means of the COOL algorithm is shown in Figure 6. The obvious problem with the fit for  $E \leq 0.1 \text{ V}$  is due to difficulties in background subtraction as discussed above.

Results from analysis of various individual voltammograms are shown in Table I. The values of  $Dt/r^2 = \theta$  corresponding to frequencies of 5, 10, 25, and 50 Hz are 0.467, 0.238, 0.093, and 0.047, respectively. At higher frequencies the component of nonplanar diffusion is so small that the resulting values of  $r$  are imprecise. This trend is reflected in the decreasing signal-to-noise ratios with increasing frequency of Table I. It is instructive to note that even for the higher values of  $\theta$  (lower frequency), the value of  $r$  is rather poorly defined by the experiment. This is not particularly surprising in that the forward and reverse currents are rather weak functions of  $\theta$ .

The COOL algorithm yields the slope of the linear regression of  $i_{exp}$  on  $\psi_{th}$  as well as the parameters of the model. From eq 2 this should be the same as the Cottrell normalizing factor. The slopes for the results of Table I are slightly lower than the Cottrell factor calculated with the independently measured values of  $D$  and  $r$ , and differ from the theoretical value by no more than 4%.

Square-wave anodic stripping voltammetry of silver. A platinum microcylinder electrode was used to perform square-wave anodic stripping voltammetry of silver with results as shown in Figure 7. The stripping peaks display a prominent shoulder at more positive potentials, the relative height of which depends on concentration. This phenomenon represents the expected behavior of such a solid deposit. A more positive potential is required to strip the final layer of silver from platinum than to dissolve the antecedent layers of silver from silver (24).

A calibration curve was constructed using peak areas as the ordinate. After establishing a baseline by connecting points on either side of the peak, the area was determined by numerically integrating the peak using the trapezoidal rule. Linear calibration curves are obtained in the  $10 \mu\text{M}$ - $1 \text{mM}$  concentration range. For example, the data of Figure 7 yield a straight line with slope  $8.89 \mu\text{A V/mM}$ , intercept  $0.086 \mu\text{A V}$ , and correlation coefficient 0.998. Lord, et al. (24) also noted considerable non-zero intercepts when stripping silver from a rotating platinum electrode (RPE). The inability to dissolve all of the silver was attributed to an interaction between silver and platinum, such as an alloy formation. The square-wave stripping curves at cylindrical electrodes display the well-known qualitative features of this system and provide analytically useful data.

ACKNOWLEDGMENT

The authors thank Mary M. Murphy for assistance.

CREDIT

This work was supported in part by the Office of Naval Research.

REFERENCES

1. Pons, S.; Fleischmann, M. *Anal. Chem.* 1987, 59, 1391A.
2. Wightman, R. M. *Anal. Chem.* 1981, 53, 1125.
3. Fleischmann, M.; Pons, S.; Rolison, D.; Schmidt, P.,  
Ultramicroelectrodes, Datatech Systems, Inc., (1987).
4. Howell, J. O.; Wightman, R. M. *J. Phys. Chem.* 1984, 88, 3915.
5. Bond, A. M.; Fleischmann, M.; Robinson, J. J. *Electroanal. Chem.*  
1984, 168, 299.
6. Howell, J. O.; Wightman, R. M. *Anal. Chem.* 1984, 56, 524.
7. Scharifker, B.; Hills, G. J. *Electroanal. Chem.* 1981, 130, 81.
8. Osteryoung, J. in Ultramicroelectrodes, Datatech Systems, Inc. (1987)  
pp 289-292.
9. MacDonald, D. Transient Techniques in Electrochemistry, Plenum Press,  
New York: 1977.
10. Aoki, K.; Honda, K.; Tokuda, K.; Matsuda, H. *J. Electroanal. Chem.*  
1985, 182, 267.
11. Aoki, K.; Honda, K.; Tokuda, K.; Matsuda, H. *J. Electroanal. Chem.*  
1985, 186, 79.
12. Aoki, K.; Honda, K.; Tokuda, K.; Matsuda, H. *J. Electroanal. Chem.*  
1985, 195, 51.
13. Sujaritvanichpong, S.; Aoki, K.; Tokuda, K.; Matsuda, H. *J.*  
*Electroanal. Chem.* 1986, 199, 271.
14. Aoki, K.; Tokuda, K.; Matsuda, H.; Osteryoung, J. *Electroanal. Chem.*  
1986, 207, 25.
15. O'Dea, J. J.; Wojciechowski, M.; Osteryoung, J.; Aoki, K. *Anal. Chem.*  
1985, 57, 954.
16. Osteryoung, J.; O'Dea, J. J. "Square-Wave Voltammetry," in A. J. Bard

- (Ed.), Electroanalytical Chemistry, Volume 14, Marcel Dekker, Inc., New York: 1986.
17. Lane, T.; O'Dea, J. J.; Osteryoung, J. G. J. Phys. Chem. 1986, 90, 2761.
  18. Delahay, P. New Instrumental Methods in Electrochemistry, Interscience Publishers, Inc., New York: 1954.
  19. Adams, R. Electrochemistry at Solid Electrodes, Marcel Dekker, Inc., New York: 1969, pp 205-208.
  20. v. Stackelberg, M.; Pilgrim, M.; Toone, V. Z. Elektrochem. 1953, 57, 342.
  21. Nelder, J. A.; Mead, R. Comput. J. 1965, 7, 308.
  22. Laitinen, H. A.; Kolthoff, I. M. J. Am. Chem. Soc. 1939, 61, 3344.
  23. Laitinen, H. A.; Kolthoff, I. M. J. Phys. Chem. 1941, 45, 1061.
  24. Lord, S. S.; O'Neill, R. C.; Rogers, B. Anal. Chem. 1952, 24, 209.

Table I. Parameters derived from square-wave voltammograms of several frequencies<sup>a</sup>.

$f$ (Hz)	$E_{1/2}^r$ (mV)	$r$ ( $\mu\text{m}$ )	$\Delta\%$	$10^4(1-R)^b$	$S/N^c$
5	218.46	11.84	5.6	3.528	117.3
10	218.50	10.79	13.6	3.195	125.6
25	219.09	12.30	1.6	8.535	79.8
50	219.53	13.54	8.0	16.54	58.6

- a) 1.19 mM  $\text{K}_3\text{Fe}(\text{CN})_6$  in 1.00 M KCl,  $r = 12.5 \mu\text{m}$ ,  $A = 0.00942 \text{ cm}^2$ ,  $E_i = 400 \text{ mV}$ ,  $\Delta E_s = 10 \text{ mV}$ ,  $E_{sw} = 50 \text{ mV}$ .
- b)  $R$  is the correlation coefficient of the line  $i_{\text{exp}} = a + b \psi_{\text{th}}$ .
- c) Signal/noise = slope(b)/ $s_i$ , where  $s_i$  is the standard deviation of the current values about the line.

## FIGURE CAPTIONS

Figure 1 - Chronoamperometric transient for 3.15 mM  $K_4Fe(CN)_6$  in 1.00 M KCl;  $A = 3.93 \times 10^{-3} \text{ cm}^2$ , potential pulsed from -100 mV to 600 mV; (O) background subtracted experiment, (-) calculation from eqns 6 and 9 (X) Cottrell equation, (o) background.

Figure 2 - Chronocoulometric transients computed from experimental chronoamperometric transients (A) and from eq 6 (B). 1.2 mM  $K_3Fe(CN)_6$  in 1.00 M KCl,  $A = 8.01 \times 10^{-3} \text{ cm}^2$ .

Figure 3 - Cyclic staircase voltammogram of 1.55 mM  $K_3Fe(CN)_6$  in 1.00 M KCl;  $A = 5.89 \times 10^{-3} \text{ cm}^2$ ,  $E_i = 500 \text{ mV}$ ,  $E_{\text{switch}} = 50 \text{ mV}$ ,  $\Delta E_s = 5 \text{ mV}$ ,  $f = 10 \text{ Hz}$ ,  $\theta = 0.467$ ; (O) experimental data, (-) calculation for planar diffusion to an electrode of the same area.

Figure 4 - Net current square wave voltammogram of 1.55 mM  $K_3Fe(CN)_6$  in 1.00 M KCl;  $A = 5.89 \times 10^{-3} \text{ cm}^2$ ,  $E_i = 500 \text{ mV}$ ,  $\Delta E_s = 5 \text{ mV}$ ,  $E_{\text{sw}} = 50 \text{ mV}$ ,  $f = 10 \text{ Hz}$ ,  $\theta = 0.234$ ; (O) experimental data, (+) calculation for planar diffusions to an electrode of the same area, (-) best fit voltammogram for planar diffusion from COOL algorithm.

Figure 5 - Frequency dependence of the net peak square wave voltammograms for 1.19 mM  $K_3Fe(CN)_6$  in 1.00 M KCl;  $A = 9.42 \times 10^{-3} \text{ cm}^2$ ,  $E_i = 400 \text{ mV}$ ,  $\Delta E_s = 10 \text{ mV}$ ,  $E_{\text{sw}} = 50 \text{ mV}$ ,  $f = 5, 10, 25, 50, 100, 200, 300 \text{ Hz}$ ; (O) normalized peak current,  $\psi/t_p^{1/2} = i/nFAC(D/\pi)^{1/2} = 0.628i$ ; (—) calculation for cylindrical diffusion, (- -) calculation

for planar diffusion. Inset: voltammograms from which the peak currents were obtained.

Figure 6 - Square-wave voltammograms for 1.19 mM  $K_3Fe(CN)_6$  in 1.00 mM KCl;  $A = 9.42 \times 10^{-3} \text{ cm}^2$ ,  $E_i = 400 \text{ mV}$ ,  $\Delta E_s = 10 \text{ mV}$ ,  $E_{sw} = 50 \text{ mV}$ ,  $f = 5 \text{ Hz}$ ,  $\theta = 0.467$ ; (O) experimental data, (-) best fit theoretical voltammogram.

Figure 7 - Square-wave anodic stripping of silver from platinum;  $A = 9.42 \times 10^{-3} \text{ cm}^2$ , conditioning potential = 500 mV, plating potential = 0 V, plating time = 15 s,  $E_i = 0 \text{ V}$ ,  $\Delta E_s = 5 \text{ mV}$ ,  $E_{sw} = 50 \text{ mV}$ ,  $f = 5 \text{ Hz}$ ,  $\theta = 0.467$ ;  $AgNO_3$  in 1.00 M  $KNO_3$ : (1) 0, (2) 10, (3) 20, (4) 30, (5) 40, (6) 50, (7) 60, (8) 70, (9) 79, (10) 89  $\mu\text{M}$ .

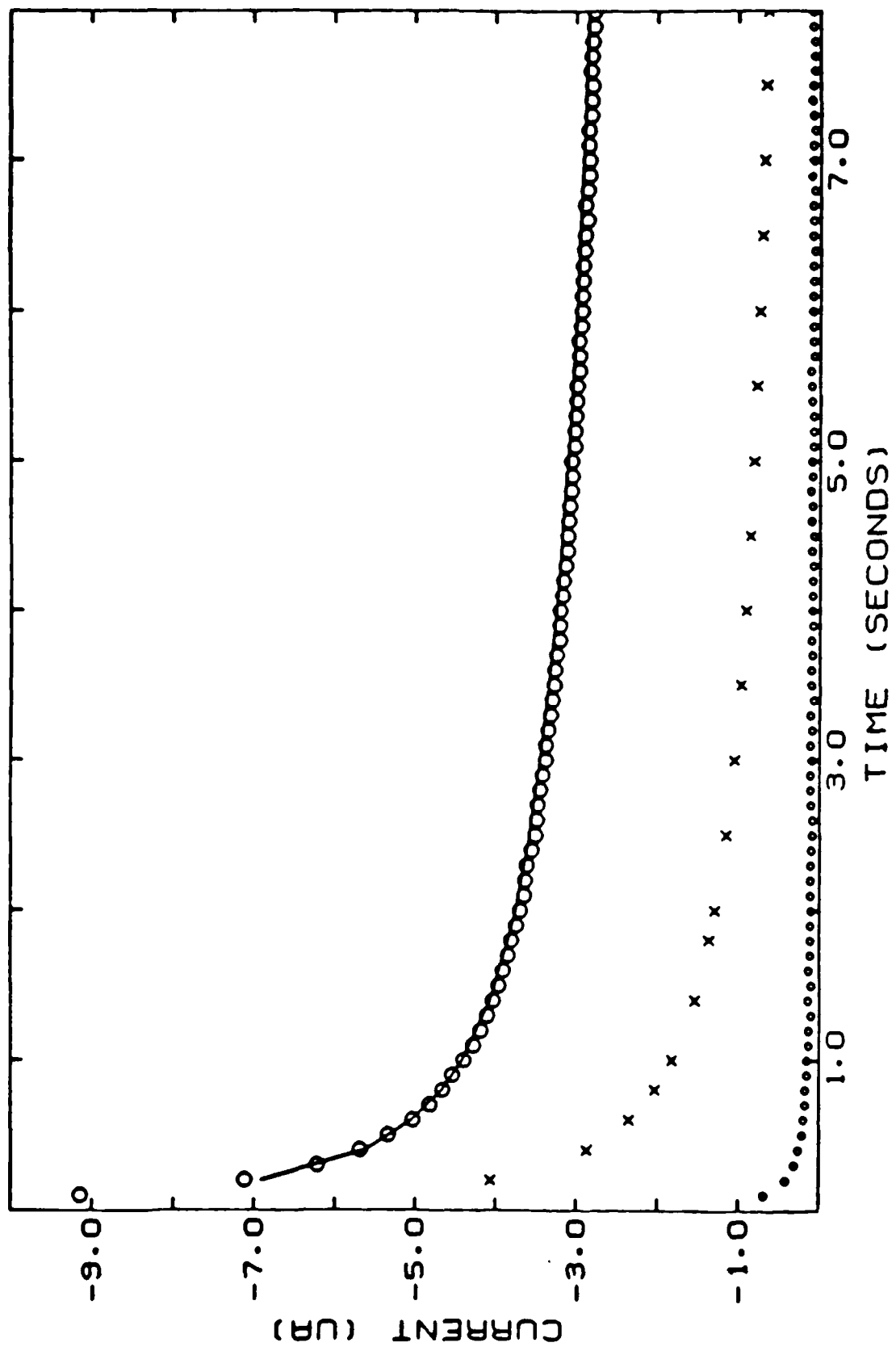


FIGURE 1

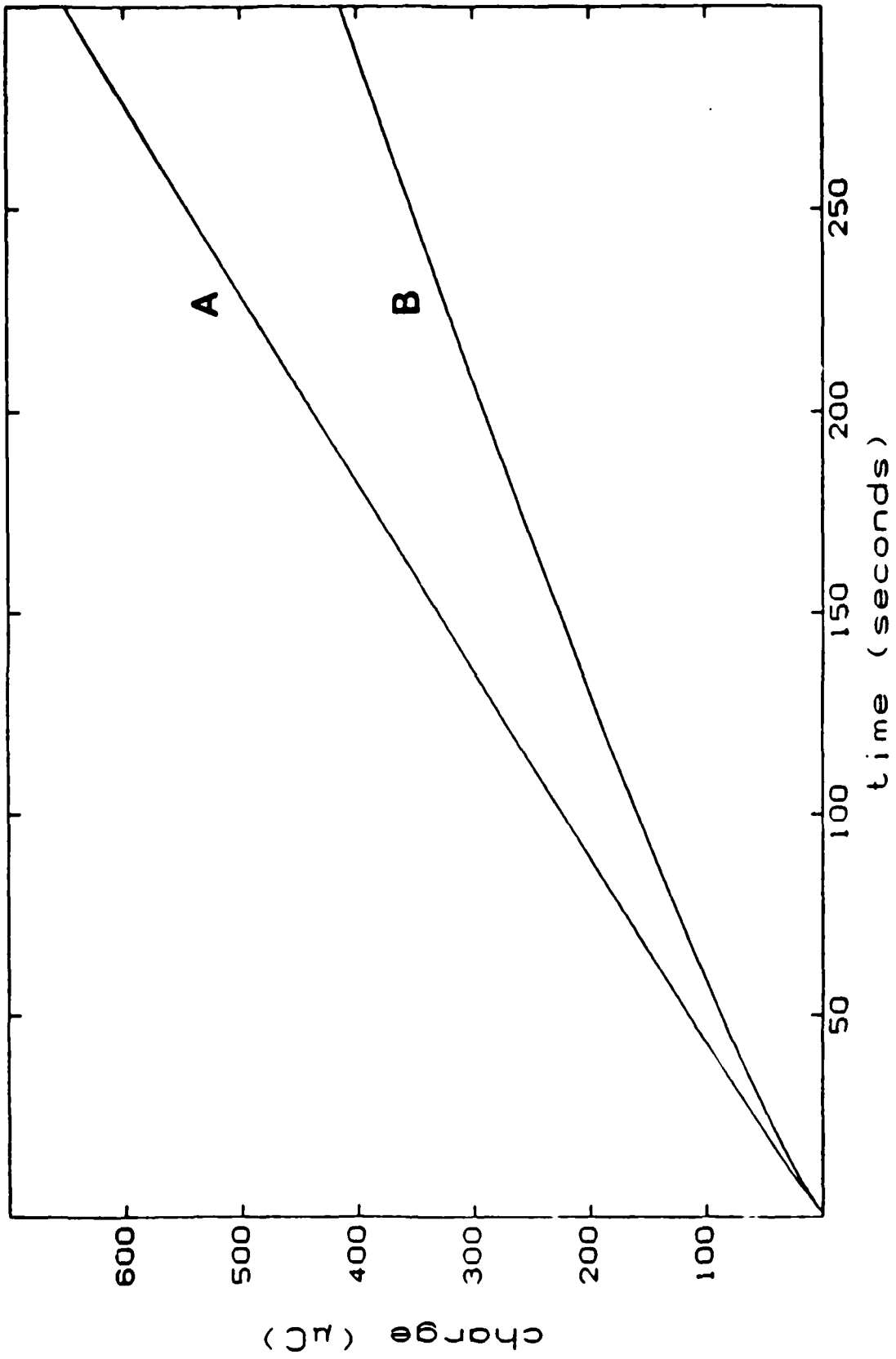


FIGURE 2

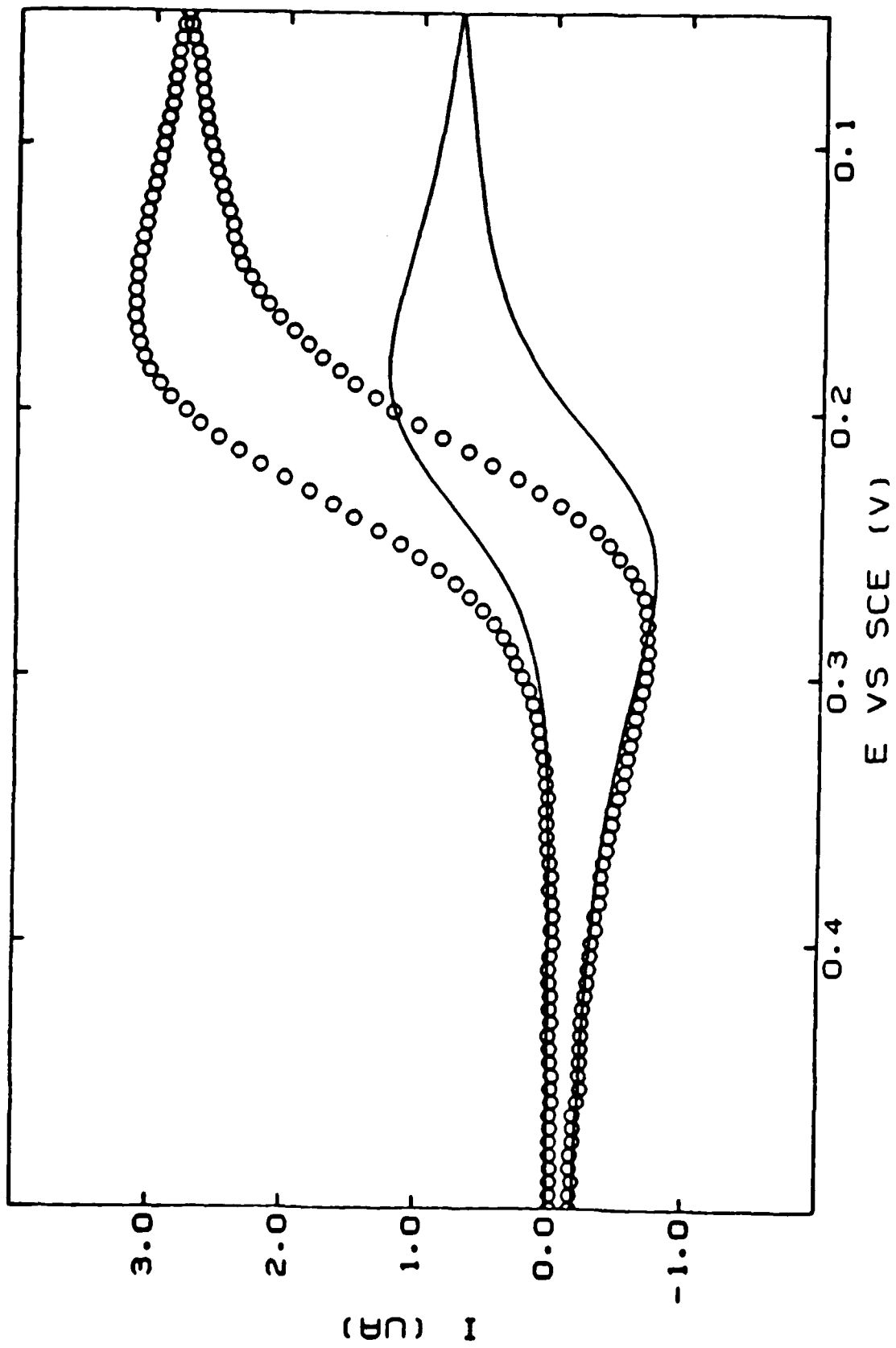


FIGURE 3

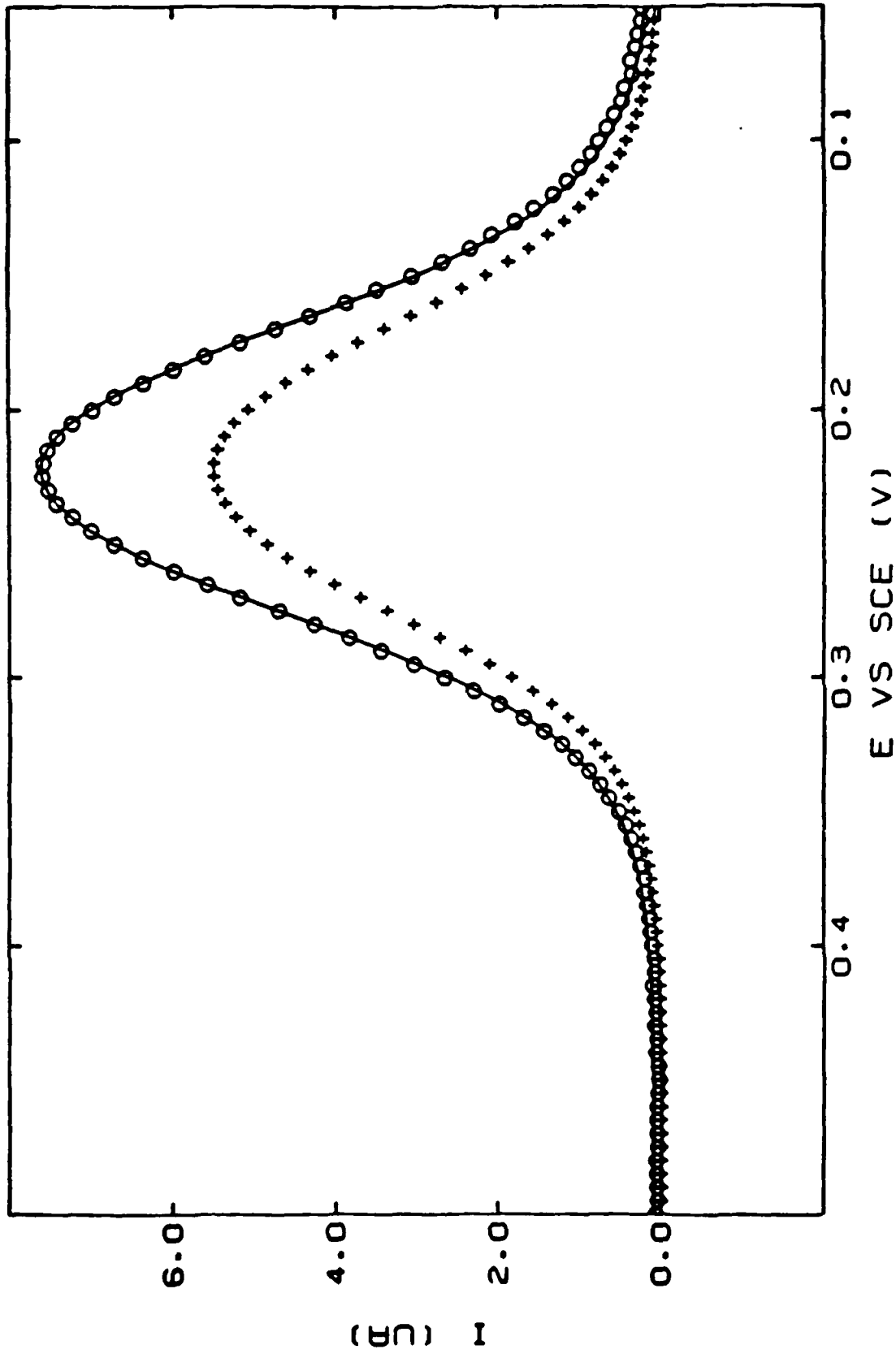


FIGURE 4

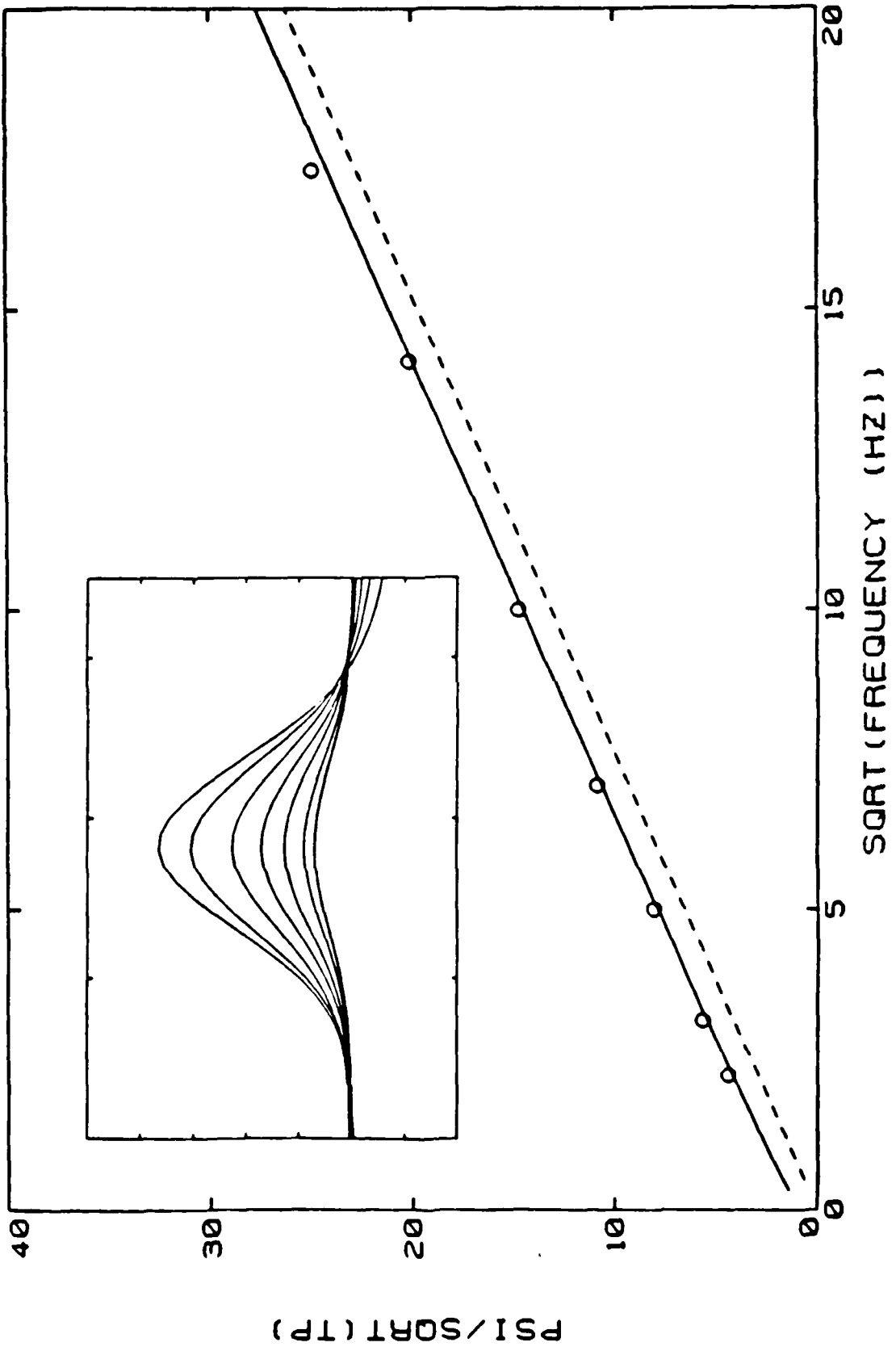


FIGURE 5

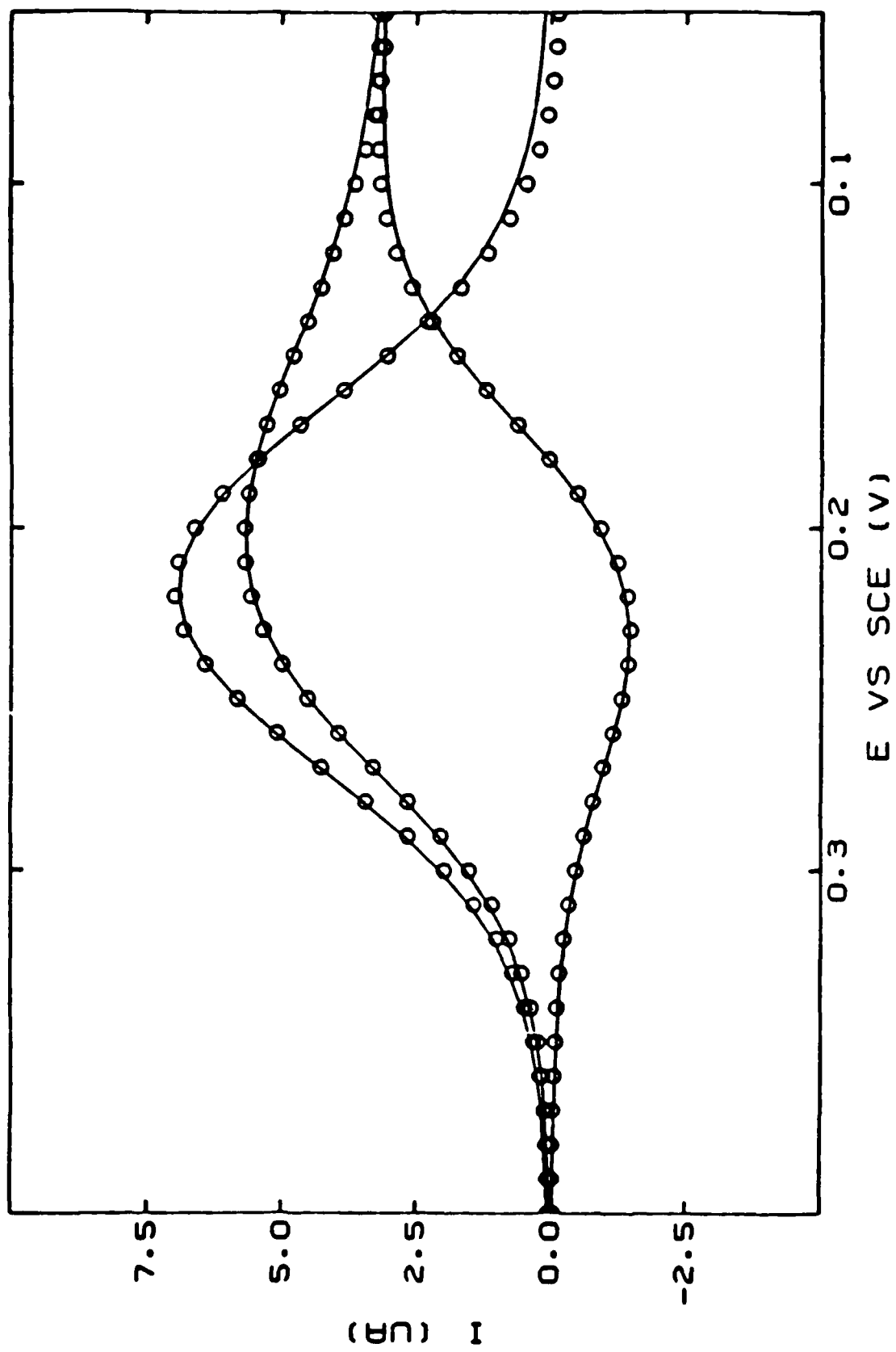


FIGURE 6

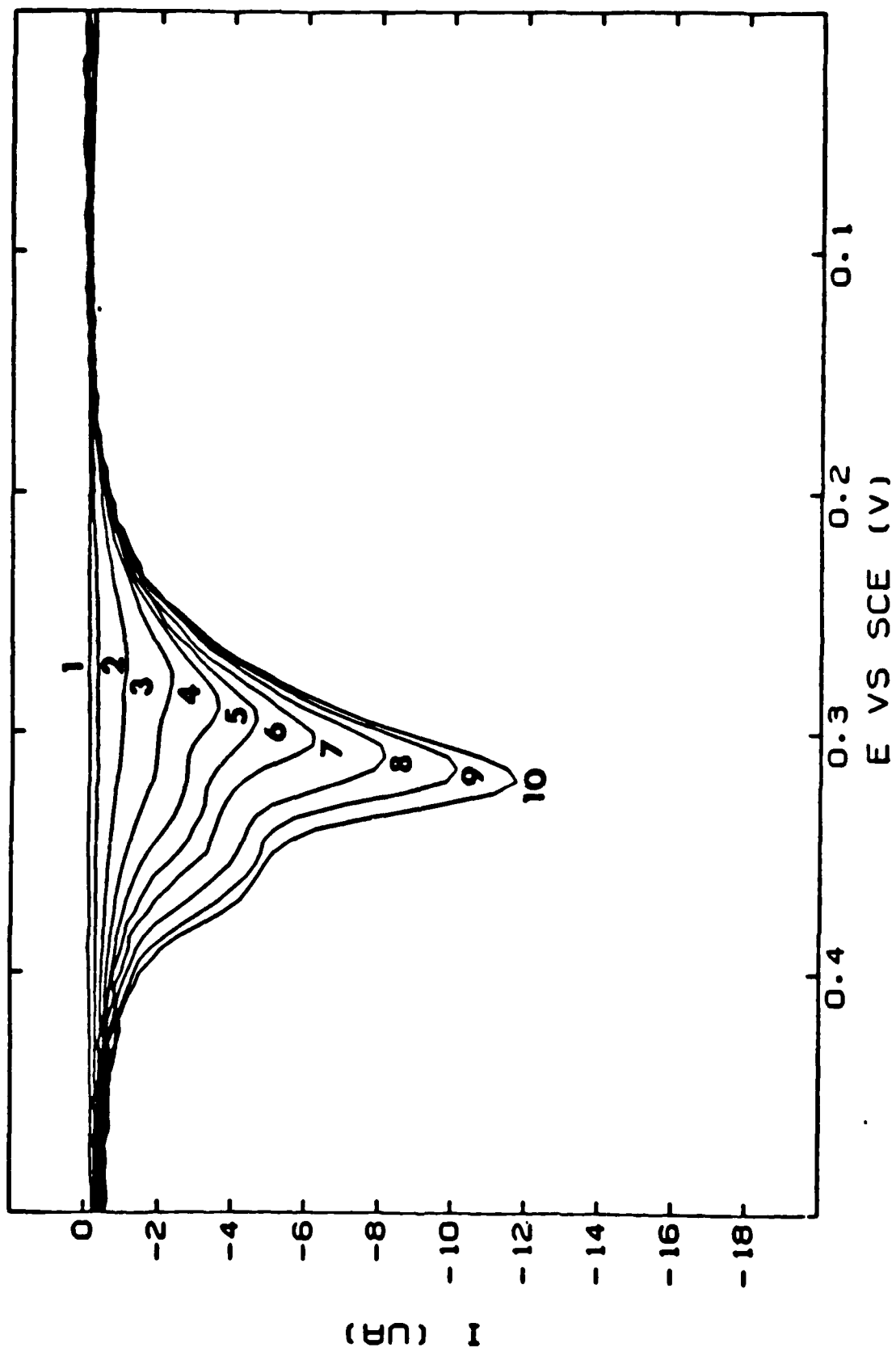


FIGURE 7

TECHNICAL REPORT DISTRIBUTION LIST, GENERAL

	<u>No. Copies</u>		<u>No. Copies</u>
Office of Naval Research Chemistry Division, Code 1113 800 North Quincy Street Arlington, VA 22217-5000	3	Dr. Ronald L. Atkins Chemistry Division (Code 385) Naval Weapons Center China Lake, CA 93555-6001	1
Commanding Officer Naval Weapons Support Center Attn: Dr. Bernard E. Doua Crane, IN 47522-5050	1	Chief of Naval Research Special Assistant for Marine Corps Matters Code OOMC 800 North Quincy Street Arlington, VA 22217-5000	1
Dr. Richard W. Drisko Naval Civil Engineering Laboratory Code L52 Port Hueneme, California 93043	1	Dr. Bernadette Eichinger Naval Ship Systems Engineering Station Code 053 Philadelphia Naval Base Philadelphia, PA 19112	1
Defense Technical Information Center Building 5, Cameron Station Alexandria, Virginia 22314	2 <u>high quality</u>		
David Taylor Research Center Dr. Eugene C. Fischer Annapolis, MD 21402-5067	1	Dr. Sachio Yamamoto Naval Ocean Systems Center Code 52 San Diego, CA 92152-5000	1
Dr. James S. Murday Chemistry Division, Code 6100 Naval Research Laboratory Washington, D.C. 20375-5000	1	David Taylor Research Center Dr. Harold H. Singerman Annapolis, MD 21402-5067 ATTN: Code 283	1